Strategy for the Measurement of Regional Cerebral Blood Flow Using Short-Lived Tracers and Emission Tomography

N. M. Alpert, *‡L. Eriksson, J. Y. Chang, †M. Bergstrom, *J. E. Litton, J. A. Correia, ‡C. Bohm, R. H. Ackerman, and J. M. Taveras

*Department of Radiology, Massachusetts General Hospital, Boston, Massachusetts, U.S.A.; Departments of *Neurophysiology and †Neuroradiology, Karolinska Institute, Karolinska Hospital, Stockholm; and ‡Department of Physics, University of Stockholm, Stockholm, Sweden*

Summary: This report describes a strategy for measurement of regional CBF that rigorously accounts for differing tracer partition coefficients and recirculation, and is convenient for use with positron emission tomography. Based on the Kety model, the measured tissue concentration can be expressed in terms of the arterial concentration, the rate constant K, and the blood flow f. The local partition coefficient may be computed as $p = f/K$. In our approach, maps of K and f are computed from two transverse section reconstructions. The reconstructions are based on weighted sums of projection data measured frequently during the observation period. Theoretical studies of noise propagation in the estimates of K and f were carried out as a function of tomographic count rate, total measurement time, and tracer half-life for varying input functions. These calculations predict that statistical errors in f of between 5 and 10% at a resolution of 1 cm full width at half maximum can be obtained with existing tomographs following i.v. injection. To compare theory and experiment, a series of flow studies were carried out in phantoms using a positron tomograph. These measurements demonstrate close agreement between computed flow and noise estimates and those measured in a controlled situation. This close agreement between theory and experiment as well as the low statistical errors observed suggest that this approach may be a useful tool in clinical investigation. **Key Words:** Emission computed tomography—Positron emission tomography—Regional cerebral blood flow—Short-lived tracers.

The measurement of regional cerebral blood flow (rCBF) using radioactive tracers and external detection has recently been coupled with emission computed tomography (ECT) to provide more accurate localization of flow in three dimensions. Two lines of methodological development have emerged: (i) equilibrium methods involving short-lived radioactive tracers and (ii) dynamic measurements. The latter approach is the subject of this article.

Dynamic methods, using inert radiolabeled gases and external detection have been used for many years to measure rCBF. Yamamoto et al. (1977) and Kanno and Lassen (1979) were among the first to apply this method with ECT. More recently, Raichle et al. (1981), Huang et al. (1982), and Carson et al. (1983) have proposed refined strategies. The strategy proposed by Huang and modified by Carson is particularly suited to ECT, since it is based on the idea of weighted projection integrals introduced by Tsui and Budinger (1978).

Several factors influence the choice of a CBF measurement strategy with ECT. Among these are the choice of a kinetic model, propagation of random and systematic error in the flow estimates, local variation in partition coefficient, and computational efficiency. All of the strategies cited above employ the Kety model (Kety, 1960), assume that a resolution-sized volume may be treated as a single compartment, and are reasonably efficient computationally. With the exception of the recent report by Carson et al. (1983), little attention has been

---

given to the statistical optimization of CBF estimators. Only the method of Huang et al. (1982) and its subsequent modification by Carson accounts for differences in local partition coefficient.

The purpose of this article is to describe a new strategy which can rigorously account for several of these factors, including recirculating tracer and differing tracer partition coefficients, but which is also computationally efficient in the production of flowmaps from transverse section data. A particularly attractive feature of our method is that the estimation of local clearance rate (but not CBF) is independent of instrument calibration factors. We present the basic theoretical foundations of the method, describe the parameter estimation procedure, describe the computational strategy, analyze the propagation of statistical noise, and present some experimental validation of the procedure and its analysis.

KINETIC MODELING

Consider a volume element of tissue, V_t, perfused with an inert, freely diffusible tracer. We wish to express the blood flow f (in ml/min/g) in V_t in terms of quantities subject to measurement by ECT and standard blood sampling techniques. The differential equation governing the tracer flow through V_t is

$$\frac{dQ}{dt} = F(C_a - \tilde{C}) - \lambda Q \tag{1}$$

where Q is the amount of radioactivity in V_t, C_a is the arterial concentration, $\tilde{C}$ is the compartment concentration, λ is the radioactive decay constant of the isotope used, and F is the arterial blood flow in ml/min. The volume of tracer distribution, V_D, and the tissue volume (V_t) under examination are not necessarily the same. Accordingly, the tomographic measurement provides a tissue concentration $C = Q/V_t$, whereas, actually, $\tilde{C} = Q/V_D$. Thus the tomographic measurements theoretically obey the equation:

$$\frac{dC}{dt} = fC_a - (\lambda + f/p)C \tag{2}$$

where we have recognized F/V_t (assuming a tissue density of one) as f, the tissue blood flow, and V_D/V_t as the partition coefficient p.

In this form, Eq. 2 is completely equivalent to the Kety theory (Kety, 1960). With the initial condition, $C(0) = 0$, Eq. 2 has the solution:

$$C(t) = f\int_0^t C_a(u)e^{k(u-t)}du \tag{3}$$

where the rate constant k is defined as $k = \lambda + f/p$.

Equation 3 treats the measured quantities C and C_a as though they were strictly deterministic. In practice, however, both C and C_a are subject to statistical fluctuations. Solutions of Eq. 3 involving experimental data will produce estimates of k and f that are subject to statistical fluctuations. To avoid further complication of the mathematical notation, we will not distinguish between the noiseless quantity and its estimator. One approach to estimating the rate constant k from the measurements is to use Eq. 3 to form the expression:

$$\frac{\int_0^T W_1(t)C(t)dt}{\int_0^T W_2(t)C(t)dt} = \frac{\int_0^T W_1(t)\int_0^t C_a(u)e^{k(u-t)}dudt}{\int_0^T W_2(t)\int_0^t C_a(u)e^{k(u-t)}dudt} \tag{4}$$

where T is the experimental observation period and W_1 and W_2 are weighting functions. As discussed later, the weights W_1 and W_2 may be chosen to minimize the variance of k. Equation 4 is particularly attractive because it yields an estimator of k that is independent of the absolute or relative quantification units of the raw concentration data. In a similar way one can obtain an expression for the estimation of f from

$$f = \frac{\int_0^T W_1(t)C(t)dt}{\int_0^T W_1(t)\int_0^t C_a(u)e^{k(u-t)}dudt} \tag{5}$$

but, it should be noted that the magnitude of f depends on the relative calibration of the tissue and arterial concentration measurements.

COMPUTATIONAL STRATEGY

Up to this stage our development has not referred explicitly to the measurement process or to tomographic imaging *per se*. Equations 1 through 5 implicitly assume that the arterial concentration history does not depend on position and that instantaneous values of the tissue concentration are available which possess infinite spatial resolution. In practice, the tissue concentrations are measured using ECT for a finite temporal sampling interval (t_s) and exhibit finite spatial resolution. Equations 1

through 5 may be applied with the understanding that $kt_s \ll 1$ and that the spatial resolution of k and f will be determined by the spatial resolution of the tissue concentration measured with ECT.

A brute force approach to the computation of blood flow parameters involves reconstruction of the tissue concentrations during the many time intervals spanning the observation period and fitting the resulting concentration data to Eq. 3. This is a potentially time-consuming process. This problem can be minimized by exploiting the equivalence between time integrals of the reconstruction values and reconstruction of time integrals of the projection data, a technique especially suited to Eqs. 4 and 5. The mathematical basis for the commutation of these summation procedures is well established and has been verified by Tsui and Budinger (1978). A practical application of this approach has been reported by Huang et al. (1982).

The operational equations, Eqs. 4 and 5, involve the tissue concentrations only as integrals of the form $\int C(t)W(t)dt$. Quantitative images of these integrals can be computed with a single reconstruction if the projection data are appropriately weighted by $W(t)$ and summed before reconstruction. Equation 4 provides the basis for a rapid, computationally efficient estimation of the rate constant. A similar equation has been used previously for computation of functional images of rCBF with ^{133}Xe using the scintillation camera (Alpert, 1977). The computational procedure involves tabulating the ratio of integrals on the right side of Eq. 4 as a function of k for a measured arterial concentration history. We call this result the R-table. For an individual experimental run, this need be done only once. The ratio of integrals of the tissue concentrations, on the left side of Eq. 4, is matched against the entries in the R-table, thereby estimating k at each picture element. For every value of k so determined the corresponding value of the denominator of Eq. 5 can also be obtained as part of the same "look-up" procedure. The end result is two quantitative images, one depicting local clearance rate and the other local blood flow. As this whole estimation procedure requires summing of the projection data (with appropriate weighting factors), two reconstructions and a table look-up procedure, its implementation can be accomplished by modification of existing reconstruction programs.

EVALUATION OF THE METHOD

Because of the Poisson nature of the radioactive decay process, the measurements of arterial and tissue concentrations are subject to statistical fluctuations, and possibly systematic errors, which propagate through the computation of k and f. For example, the shape of the arterial input function, the physical half-life of the tracer, and the duration of the measurement period influence the magnitude of the fluctuations in k and f. The properties of this method have been studied both theoretically and experimentally. The following sections describe the methods and results of these studies.

Theoretical evaluation

To study theoretically the effect of these experimental factors, we treated the tomographically determined concentrations as statistically independent (temporally), random variables. All calculations were made for a simple physical model consisting of spatially and temporally uniform fluid flow through a disk 15 cm in diameter. For purposes of computation, a single-slice tomograph was assumed with a spatial resolution of 1 cm full width at half maximum (FWHM), capable of recording a maximum useful count rate of 50,000 coincidence events per second. To simplify the calculations, we neglected deadtime effects and the noise contribution due to fluctuations in the arterial concentration measurements. The weighting factors W_1 and W_2 were chosen to be 1 and t, respectively, yielding the maximum likelihood estimator of k in the limiting case with Poisson statistics, spike injection, no recirculation, and no transverse section reconstruction. The variances, denoted by σ^2, in k and f were approximated by a Taylor series expansion retaining first-order terms (Meyer, 1975) and given by the following expressions:

$$\sigma^2(k) = \sum_{i=1}^{n} \left(\frac{\partial k}{\partial C_i} \right)^2 \sigma^2(C_i) \qquad (6)$$

and

$$\sigma^2(f) = \sum_{i=1}^{n} \left(\frac{\partial f}{\partial C_i} + \frac{\partial f}{\partial k} \frac{\partial k}{\partial C_i} \right)^2 \sigma^2(C_i) \qquad (7)$$

where $t_i = i \cdot t_s$, $t_s = T/n$, and $C_i = C(t_i)$.

Because we have assumed spatially uniform flow, the variance of the concentration in the disk with uniform flow can be shown to be separable into two factors: (i) a time-dependent part and (ii) a factor which varies spatially. In our calculations the factor that varies spatially was computed analytically for the center of the disk and includes the effects of photon attenuation (Alpert et al., 1982). The time-dependent factors were computed for spike (delta function) and a simulated i.v. injection. For the spike injection calculations it was assumed that maximum instantaneous count rate of 50,000 events per second was achieved. Delta function injections were weighted by a factor $1/f$, so that the total activity injected was the same in all cases.

For the simulated i.v. injection, lower count rates would be expected for the same quantity of injected radioactive tracer; the concentration variances, therefore, were normalized according to the calculated concentration history.

Equation 8 shows the expression used to simulate an i.v. injection:

rough the
ipe of the
the tracer,
luence the
properties
ically and
cribe the

$$C_a(t) = \frac{C_0}{f}[20 \cdot t \cdot e^{-10t} + 0.025 \cdot f \cdot (1 - e^{-0.9t})]e^{-\lambda t}$$

(8)

Equation 8 is not based on physiological measurement, but rather was constructed for the purpose of these calculations. The first term in Eq. 8 was used to approximate the initial passage of a bolus through a volume element. Conservation of tracer mass was invoked to normalize the amount of tracer entering the disc on the first pass to 20% of that used in a spike injection. This normalization procedure was used to simulate the lower concentrates that would be observed with i.v. injection, assuming that the total activity was fixed in all cases. The factor of f^{-1} arises from this procedure because the total activity is given by $F\int C_a(t)dt$. The second term approximates the effect of tracer recirculation and dilution in the total body volume of distribution.

erimental
ined con-
iporally),
r a simple
orally uni-
ieter. For
raph was
width at
g a max-
vents per
ted dead-
ctuations
its. The
: 1 and t,
estimator
spike in-
ction re-
i k and f
retaining
following

To obtain values of $\sigma^2(k)$ and $\sigma^2(f)$, Eqs. 6 and 7 were programmed in a digital computer. Equations 4 and 5 were recast as discrete sums and differentiated to obtain analytic expressions for $\partial k/\partial C_i$ and $\partial f/\partial C_i$. Time sampling of the tissue and arterial concentrations was kept constant in the calculations at 5 s. Numerical integrations of the form

$$\int_0^t C_a(u)e^{k(u-t)}du$$

were performed using the IMSL subroutine DCADRE.

(6)

The results of simulation studies based on this approach are summarized in Figs. 1–6. They show the calculated effects of measurement time, decay constant, and shape of the input function on the noise in K and f. It should be noted that K differs from k, where $k = K + \lambda$ and $K = f/p$. These data are presented as fractional errors, denoted by E. They represent one standard deviation of the quantity divided by its expected value. Figure 1 shows the $E(K)$ (fractional error in K) versus K for measurement periods of 1, 2, 4, and 10 min, assuming a spike injection with no recirculation and no radioactive decay (i.e., $\lambda = 0$). Figure 2 shows the increased fractional error in K resulting from the use of the short-lived tracer ^{15}O with $\lambda = 0.335$ min^{-1}. Figure 3 is analogous to Fig. 1, showing $E(K)$ versus K, but assuming a simulated i.v. injection with recirculation and $\lambda = 0.335$ min^{-1}. Figure 4 shows $E(f)$ (fractional error in f) versus f, assuming $\lambda = 0.335$ min^{-1}, a spike injection and no recirculation. Figure 5 shows the same basic situation, but assumes a simulated i.v. injection with recirculation. Figure 6 again shows $E(f)$ versus f but assumes no radioactive decay (i.e., $\lambda = 0$).

(7)

Experimental evaluation

low, the
uniform
ors: (i) a
ies spa-
spatially
lisk and
rt et al.,
ated for
ion. For
iat max-
nts per
is were
injected

it rates
cted ra-
erefore,
icentra-

ilate an

Measurements in a phantom were undertaken to allow comparison of theory and experiment in a controlled situation. The phantom consisted of a spherical flask 7.8 cm in diameter and a motor-driven stirring system. During the experiments, water was pumped continuously through the phantom via a single inlet and a single outlet. Rapid mixing in the flask was facilitated by continuous stirring of the liquid with a motor-driven paddle at about 30 revolutions per minute. Radioactivity was introduced into the sphere via a rapid injection approximating a delta
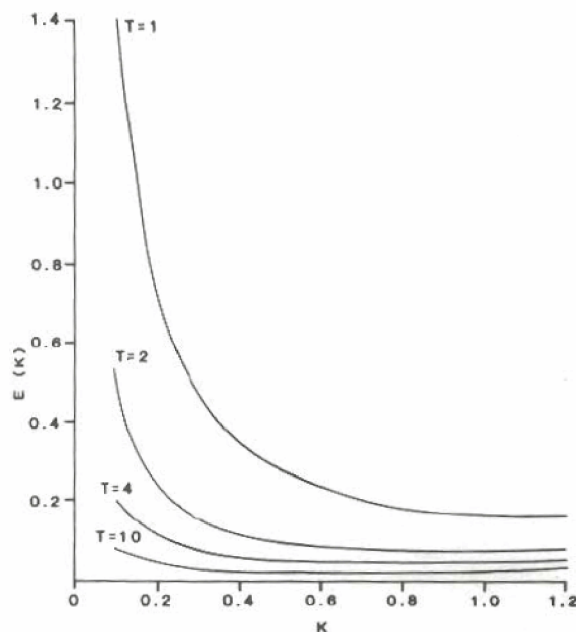

FIG. 1. The fractional error in K versus K due to statistical fluctuations in tissue concentration data, for $\lambda = 0$, $p = 1$, a spike injection, and no recirculation. Separate calculations are shown for measurements periods (T) of 1, 2, 4 and 10 min.

function. No recirculation of tracer was permitted. Total flow through the phantom was estimated from the volume of the effluent and the elapsed time. The reference value of the rate constant was determined by dividing the total flow by the volume of distribution, i.e., the fluid volume of the phantom.

Sequential tomographic measurements were made with the Karolinska Institute positron emission tomograph
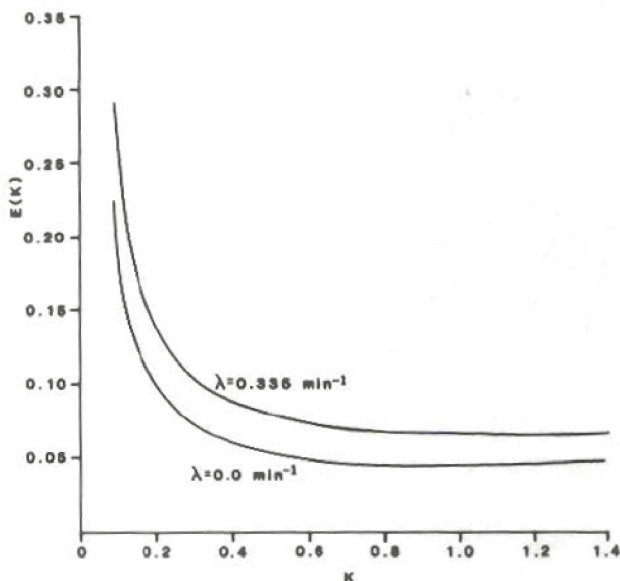

FIG. 2. Effect of radioactive decay and measurement time on fractional error in K. All parameters are as for Fig. 1, except $\lambda = 0.335$ min^{-1} and $T = 4$ min.
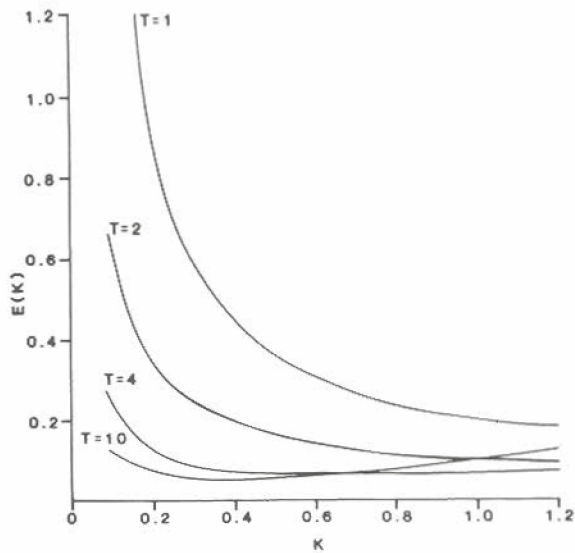
FIG. 3. Effect of bolus shape and measurement time on fractional error in K. For these calculations, $\lambda = 0.335$ min^{-1} and a simulated i.v. injection history (see text for details) was used.

(Scandatronix-PC384) following injection of 0.5–2.0 mCi Ga-68 EDTA into the phantom. Data were collected for observation periods of 100 or 200 s in frames of 10-s duration. The data were used to produce a map of K values, as described above, by table look-up. Figure 7 shows one such map, in which $K = 0.87$ min^{-1}. The central region, 3 cm in diameter, of each disk-shaped map was examined to determine the average K value and its fractional error. The results of the tomographic measurements are presented in Table 1, along with the values determined from the effluent-measurement time relationship (ratio of pump output rate to phantom volume). The duration of data collection for the six runs shown in Table 1 was 200 s for
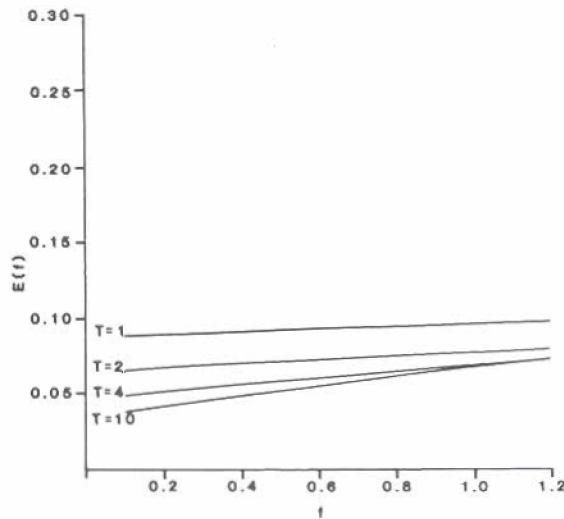

FIG. 4. The fractional error in f versus f due to statistical fluctuations in tissue concentration data. The calculations assume $\lambda = 0.335$ min^{-1}, $p = 1$, spike injection, and no recirculation. Separate calculations are shown for measurement periods of 1, 2, 4, and 10 min.
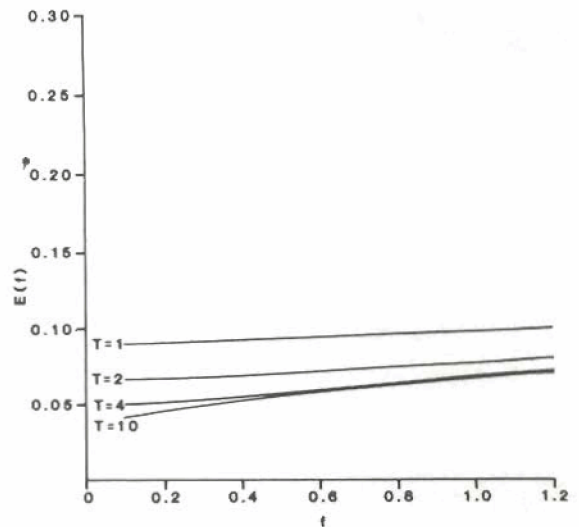
FIG. 5. Effect of bolus shape and measurement time on fractional error in f. All parameters are as for Fig. 4, but a simulated i.v. injection history (see text for details) was used.

run 1 and 100 s for the others. The expected value of the fractional error in K calculated with the formalism discussed above was found to be in good agreement with the fractional errors computed from the flow maps. It was not possible to obtain flow estimates from these experiments. Therefore, formal evaluation of Eq. 5 is a subject for future work.

DISCUSSION AND CONCLUSIONS

An underlying assumption in our work is that the tomographically defined tissue volume is homogeneous. With tomographic resolution on the order of 1 cm^3, this assumption is, at best, only approximately satisfied. Further, the Kety model on which our work is based treats capillary and surrounding tissue as a unit. No attempt is made to model details such as transport limitations imposed by the per-
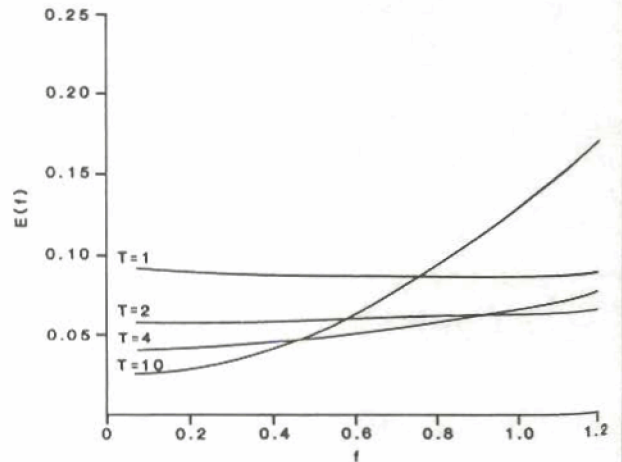

FIG. 6. Effect of long tracer half-life and measurement time on fractional error in f. All parameters as for Fig. 5, but $\lambda = 0$.
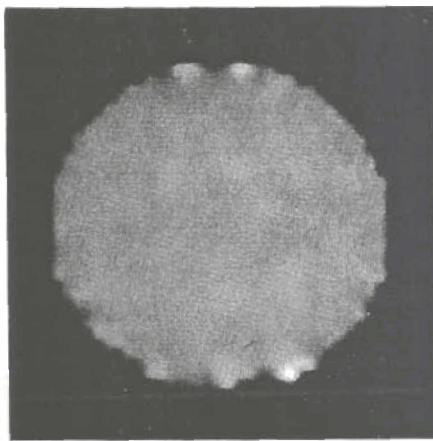
FIG. 7. Map of local clearance rate measured on a transverse section through a 7.8-cm-diameter spherical phantom. $K = 0.87 \pm 0.04$ min^{-1}. The resolution of the underlying local concentration values was approximately 8 mm FWHM (in-plane). The initial prompt coincidence rate was 35×10^3 cps.

meability of the cell membrane to specific tracers. Thus, the current approach and other work, which similarly lump tissue properties, will typically produce a locally averaged blood flow. In the future, when higher-quality tomographic data become available, they may support analyses with more than one compartment or possibly with more detailed and realistic kinetic models.

This article describes an analytic solution to the problem of estimating the rate constant and blood flow parameters from experimental data. Although the partition coefficient is not explicitly estimated, differences in local partition coefficient are automatically accommodated by this approach. If desired, the partition coefficient can be determined directly from the equations presented above. The ideal estimation procedure, in a statistical sense, would compute minimum variance estimators for these parameters. This ideal must be balanced against the need to analyze flow through many tissue elements, and perhaps to display the results as perfusion maps. To study the possibility of using minimum variance estimators, we approximated $\sigma^2(K)$ by Eq. 6. Using Eq. 4 in the form of a discrete sum with m elements, to determine K one can treat

$\sigma^2(K)$ as a function of $2 \times m$ values of W_1 and W_2 for a given set of arterial and tissue concentrations. It is then a straightforward matter to minimize $\sigma^2(K)$ with respect to the W_1 values and W_2 values. This procedure yields coupled nonlinear equations for each pixel. The rapid solution of these equations at each pixel would require the application of considerable computational resources. Although the estimators used in our method reduce to the maximum likelihood solution in certain limits (Alpert, 1977), it is not possible to say how close to the theoretical optimum they may be.

The noise propagation calculations presented above are for a physical rather than a physiological flow model. Nevertheless, if properly interpreted, we believe these results can be of help in designing experimental protocols. The 15-cm-diameter disk with uniform fluid flow was intended to provide a highly simplified representation of brain blood flow. As with static activity distributions (Budinger et al., 1977), the disk with uniform distribution of fluid flow may serve as a standard for comparing the level of statistical noise in local blood flow estimates. In brain, regional blood flow is known to vary by at least a factor of two between white and gray matter structures. Because of the uniform flow, the disk model is likely to exaggerate the effect of statistical noise propagated by the reconstruction procedure when compared to *in vivo* measurements. It is recognized that the combination of tomographic resolution, count rate capability, and sensitivity assumed in our calculations may not be representative of any tomograph available today. In such cases, the results of our calculations can be modified using the equation shown below so that they more closely represent the experimental situation.

$$E_{new} = E_{old} \times 224 \, (CR)^{-1/2} \, R^{-3/2} \qquad (9)$$

where E is the fractional error in K or f, R is the tomographic resolution, and $(CR)_{max}$ is the maximum count rate in the proposed experiment.

The results shown in Fig. 1 illustrate several general points relative to the statistical precision of clearance rate measurements: (i) $E(K)$ versus K tends to infinity at $K = 0$. Additional calculations have shown that $E(K)$ falls as K increases, eventually reaching a minimum and then rises monotonically. (ii) Increasing the measurement period reduces the fractional error more at low K than at high K. (iii) Without the confounding effects of bolus shape, recirculation and radioactive decay increasing the measurement period is a useful strategy for reducing the variance in estimates of K.

TABLE 1. *Results of tomographic measurements*

Run	Reference K (min^{-1})	Measured K (min^{-1})	SD
1	0.09	0.08	0.03
2	0.17	0.17	0.11
3	0.29	0.27	0.16
4	0.63	0.61	0.04
5	0.88	0.87	0.04
6	1.03	1.06	0.05

The influence of the time course (shape) of the injection history for finite injections is illustrated in Fig. 3. These data are directly comparable to Fig. 1 in that it was assumed that the same total activity was injected at time zero. The curve parameters in Eq. 8 were chosen such that 20% of the total activity entered the phantom in the initial bolus; later, the concentration assumes a level governed by the dilution in the total volume of distribution. Overall, the shapes of the fractional error curves are similar to those computed for spike injection. Only a modest increase in the relative error in K is predicted for the i.v. relative to the nonrecirculating spike injection. Furthermore, as the measurement period is increased beyond about 4 min, a tendency toward noise amplification at high K values may be observed. This tendency results from the fact that the shape of the injection function at later times varies only due to radioactive decay.

Figure 4 shows graphs of the $E(f)$ as a function of f. There is a progressive increase in the relative error in f as the observation period is reduced. For a given observation period, the relative error decreases (but does not go to zero) with decreasing flow. For the same injected activity at high flows, the relative error in f cannot be reduced by increasing the measurement time. For comparison, Fig. 5 shows $E(f)$ versus f assuming an i.v. injection. All the other parameters were the same as those used in the calculations shown in Fig. 4. The i.v. error curves exhibit the same general behavior as those for the spike injection, and the overall noise level differs only slightly.

The most important observations from these calculations are contained in Figs. 4 and 5, which pertain most directly to measurements with tracers such as [^{15}O]H$_2$O. The calculations predict the magnitude of the fractional error to be between 0.05 and 0.10 for the physiological range of flow values. It should be noted that for the shorter measurement periods of 1 and 2 min, $E(f)$ varies only slightly with f. For longer measurement periods there is a tendency to noise amplification at higher flow values. This noise amplification can be better appreciated from the calculation of Fig. 6. All the conditions were the same as those for the previous calculations, except that the decay constant was set to zero. Inspection shows that the differences are minor for the shorter measurement periods, but for $T = 4$ and $T = 10$, a tendency toward considerable noise amplification is seen. This noise amplification suggests that the data measured late in the experiment, when the input function is changing slowly, are being weighted too heavily. For studies with i.v. injection, the weighting factors W_1 and W_2 should be reduced as time progresses. The optimum func-

tional form of these weights is a question for future study.

The experimental validation studies reported in this article provide a useful cross-check and touchstone between the theoretical developments and experimental measurement. The use of a physical phantom rather than a biological system allows for controlled comparisons in situations close to the theoretical ideal. Table 1 shows that excellent agreement was obtained between experiment and the reference values of the rate constants. This close agreement between theory and experiment provides an initial validation of this approach. Furthermore, the low statistical errors measured in the flow maps, even after extrapolating to head-sized objects, suggests that this approach to measurement of rCBF may be useful in both animal and clinical investigations. In addition, statistical analyses showed that the fractional errors in K were closely predicted with the formalism presented above.

REFERENCES

Alpert NM (1977) Functional imaging. In: Computer Methods. (Lieberman DG, ed), St. Louis, CV Mosby, pp 139–147
Alpert NM, Chesler DA, Correia JA, Ackerman RH, Chang JY, Finklestein S, Davis SM, Taveras JM (1982) Estimation of the local statistical noise in emission computed tomography. IEEE Trans Med Imaging MI-1:142–146
Budinger TF, Derenzo SE, Gulberg GT, Greenberg WL, Huesman RH (1977) Emission computer assisted tomography with single-photon and positron annihilation emitters. J Comput Assist Tomogr 1:131–145
Carson RE, Huang SC, Phelps ME (1983) Optimization of the O-15 water bolus injection technique for quantitative local cerebral blood flow measurements using positron emission tomography. J Cereb Blood Flow Metabol 3(Suppl 1):S11–S12
Huang SC, Carson RE, Phelps ME (1982) Measurement of local blood flow and distribution volume with short-lived isotopes: a general input technique. J Cereb Blood Flow Metabol 2:99–108
Kanno I, Lassen NA (1979) Two methods for calculating regional blood flow from emission computed tomography of inert gas concentrations. J Comput Assist Tomogr 3:71–76
Kety SS (1960) Measurement of local blood flow by the exchange of an inert, diffusible substance. Methods Med Res 8:228–236
Meyer S (1975) Data Analysis for Scientists and Engineers. New York, J Wiley & Sons, p 39
Raichle ME, Markham J, Larson K, Grubb RLJ, Welch MJ (1981) Measurement of local cerebral blood flow in man with positron emission tomography. J Cereb Blood Flow Metabol 1(Suppl 1):S19–S29
Tsui E, Budinger TF (1978) Transverse section imaging of mean clearance time. Phys Med Biol 23:644–653
Yamamoto YL, Thompson CJ, Meyer E, Robertson JS, Feindel W (1977) Dynamic positron emission tomography for study of cerebral hemodynamics in a cross section of the head using positron emitting ^{68}Ga-EDTA and ^{77}Kr. J Comput Assist Tomogr 1:43–45